Strojniški vestnik - Journal of Mechanical Engineering 55(2009)10, 590-598
UDC 669.14.018.8
Paper received: 08.04.2009
Paper accepted: 25.09.2009

Numerical Simulation of Stress Relieving of an Austenite Stainless Steel

Janez Urevc[1,*] - Pino Koc[2] - Boris Štok[1]
[1] University of Ljubljana, Faculty of Mechanical Engineering, Slovenia
[2] University of Ljubljana, Faculty of Mathematics and Physics, Slovenia

An approach to numerical simulation of the annealing process with stress relieving is presented in the paper. For austenite stainless steel 316L (AISI), which exhibits no phase transformation from the melting point to room temperature, a viscous-elastic-plastic constitutive model is elaborated. First, from given experimental data the respective mechanical material parameters as a function of temperature are numerically identified by an inverse procedure. Then, the adequacy of the adopted model and identified material parameters is proven by a numerical simulation of stress relieving in two technological cases: (i) two-stage deep drawing with intermediate stress annealing and, (ii) simplified welding process followed by post weld heat treatment. In both cases the obtained residual stress state reduction is found to be in good agreement with the empirical experience and data provided from literature.

Keywords: mechanical properties, modelling and process simulation, stress relieving, viscous-elastic-plastic constitutive model, stainless steel

0 INTRODUCTION

The importance of heat treatment in modern technology can be demonstrated by the fact that a significant amount of machine and structural components are subject to at least one heat treatment process in their manufacture, which is usually one of the final production operations. In order to modify the actual physical and mechanical properties of a metal or alloy in the solid state any heat treatment process involves controlled heating and cooling. Implied thermal changes may be essential to improve the processing of the worked part (e.g. machinability) or to meet proper service conditions (e.g. increased surface and core hardness, wear and dimensional accuracy, residual stress profile and desired microstructure, improvements of toughness, ductility, weld integrity, etc.) [1]. Heat treatment techniques include normalizing, case hardening, tempering, quenching and annealing. The purpose of the latter, which is addressed in this paper, is to relieve the residual stresses from a heat treated component, arisen during previous manufacture history.

When steels are subject to cold-working, heat treatment or welding the residual stresses are inevitably introduced into the processed parts. To reduce the level of residual stresses to a reasonable small value without (un)intentionally changing the microstructure and mechanical properties of a material, the usual practice is to provide stress-relief annealing [2]. The process is typically applied to metal forming products where a high degree of plastic deformation is accumulated (hot or cold forgings, rolled sheets, drawn parts, etc). Sometimes stress-relief annealing is also used to reduce by welding induced high residual stresses, which can seriously affect service performance of a welded structure [3]. The disadvantage of heat treatment is mainly associated with high cost, particularly in regard to the necessary equipment and also, because of the required large heating times, great energy consumption. Thus, any effort made to reduce the respective costs is always welcome. From the point of view of process design, modern finite element method (FEM) based analysis tools can be of great help, in particular when attempting to find optimal process parameters with regard to both, the required product quality and cost effectiveness.

One of the key problems of heat treatment numerical simulations is material modelling. Namely, in order to be physically objective the numerical simulations of heat treatment require the use of proper material constitutive model with a consistent set of temperature dependent material data. A survey of related literature [4] to [7] shows that different material models have been used to tackle the heat treatment simulation problem. Ronda and Oliver [4] investigated the

*Corr. Author's Address: University of Ljubljana, Faculty of Mechanical Engineering, Aškerčeva 6, SI-1000 Ljubljana, Slovenia, janez.urevc@fs.uni-lj.si

applicability of several thermo-viscous-plastic models to assess the final residual stress state in the case of welding simulation. Based on the established quantitative difference between different constitutive models their study indicates that the material constitutive law must be chosen with care. Simulations of post welding heat treatment have been carried out by Josefson [7], who calculated the residual stresses of a thin wall pipe after post weld heat treatment. Wang [5] simulated local post heat treatment of a pipe with the use of a power creep law. A comparison of the numerical simulation results of welding and stress relief heat treatment for five constitutive models was done by Alberg and Berglund [6]. They found that the cooling stage of post weld heat treatment process did not cause any additional plastic strains and that the choice of a creep model has only a minor effect on the residual stresses in the heat treatment simulation – which is somewhat different to the study made by Ronda and Oliver [4]. Berglund et al. [8] simulated the stress relief heat treatment after a welding process employing Norton's law [9]. They also concluded that no additional plastic strain is produced in the cooling stage of heat treatment.

The importance of the viscous part in the material behaviour is emphasized in works [4], [5] and [9], where accordingly complete constitutive models including all three rheological modes (viscosity, elasticity and plasticity) have been presented. But when data on viscous behaviour are not available, Depradeux and Jullien [10] indicate that kinematic material hardening should be used.

The aim of this paper is to assume viscous-elastic-plastic material behaviour with a corresponding constitutive law that would enable physically reliable numerical simulation of the stress relief heat treatment. The material of our interest is austenite stainless steel AISI 316L. The necessary material data for the adopted constitutive model are determined using the inverse identification method on an experimental data base extracted from a published source [10]. The validation of the performed material characterization is based on a comparison with the results from literature [11]. The applicability of the developed numerical heat treatment model is demonstrated by considering two cases: (i) two-stage sheet metal forming process with intermediate stress relieving and, (ii) heat treatment after arc heating (process used for local heating of the material, similar to welding but without added filler material).

1 CONSTITUTIVE MODEL

Although a sequentially coupled approach, with mechanical analysis performed after the complete temperature evolution has been computed from the thermal analysis separately is considered sufficient for heat treatment processes [11], in our work the stress relieving phenomenon is treated in a fully coupled way using a staggered procedure [12]. The coupled analysis is used whenever the thermal and mechanical fields affect each other strongly, i.e. when the stress evolution is dependent on temperature distribution and temperature evolution depends on mechanical energy dissipation [11]. Numerically, the stress/displacement and temperature fields are solved iteratively by applying increments of mechanical load and temperature change alternatively, thus giving an impression of simultaneously solving both problems. The mathematical model includes two phenomena, the thermal and the mechanical one, both of which are incorporated into the model in a basic form of the balance of internal energy and the balance of momentum.

In ABAQUS [13], the FEM code used in our work to numerically treat the considered non-linear thermal-stress problem, the system of equations resulting from the coupled approach is solved using Newton's method. An exact implementation of Newton's method involves a nonsymmetric system matrix

$$\begin{bmatrix} K_{uu} & K_{uT} \\ K_{Tu} & K_{TT} \end{bmatrix} \begin{Bmatrix} \Delta u \\ \Delta T \end{Bmatrix} = \begin{Bmatrix} R_u \\ R_T \end{Bmatrix}, \tag{1}$$

where K is the system matrix. This matrix is partitioned into four submatrices: the stiffness matrix K_{uu} corresponding to the mechanical part of the coupled problem; the matrix K_{uT} giving transformation of the thermal energy into the mechanical one; the matrix K_{Tu} giving transformation of the mechanical energy into the thermal one and the thermal matrix K_{TT} which is assembled from considering conduction and convection parts. The primary physical variables of the problem are the displacement vector field u and the temperature scalar field T. In the context

of discrete analysis they are written in Eq. (1) in the nodal incremental vectorial form Δu and ΔT. The right hand side of Eq. (1) consists of the vectors R_u and R_T, the mechanical residual vector and the thermal flux residual vector, respectively. Primarily, those vectors represent the externally applied nodal mechanical and thermal loads, as well as consequences of internal stresses and heat generation. Apart from that, the considered problem being nonlinear and physically coupled, those vectors take into account also the numerical departure from the equilibrium state at any stage of the iteration procedure.

1.1 Mechanical Governing Equation

The material behaviour is mechanically manifested with the respective deformation, the total strain rate tensor $\dot{\boldsymbol{\varepsilon}}$ being defined as a sum of individual constituent rheological parts

$$\dot{\boldsymbol{\varepsilon}} = \dot{\boldsymbol{\varepsilon}}^{e} + \dot{\boldsymbol{\varepsilon}}^{th} + \dot{\boldsymbol{\varepsilon}}^{ie} = \dot{\boldsymbol{\varepsilon}}^{e} + \dot{\boldsymbol{\varepsilon}}^{th} + \dot{\boldsymbol{\varepsilon}}^{pl} + \dot{\boldsymbol{\varepsilon}}^{cr}. \quad (2)$$

Superscripts *e*, *th* and *ie* in Eq. (2) represent respectively strain rates due to elastic, thermal and inelastic response. The latter can be further decomposed into plastic and creep part. Elastic strain follows Hooke's law, plastic behaviour with isotropic hardening obeys von Mises yield rule whereas thermal strain rate is a product of thermal expansion coefficient and temperature rate. Creep strain rate representing the viscous part of the material behaviour in the secondary or steady-state creep phase [13] is defined in accordance with equivalent uniaxial behaviour. We assume that uniaxial equivalent creep strain rate $\dot{\varepsilon}^{cr}$ is governed by a power law model

$$\dot{\varepsilon}^{cr} = A \cdot \tilde{q}^{n} \cdot t^{m}, \quad (3)$$

where A, n and m are temperature dependent material properties, $\tilde{q}$ is the uniaxial equivalent deviatoric stress and t the elapsed time from the creep initiation. To estimate material properties A, n and m a series of uniaxial tension experiments under different strain rates at different temperatures needs to be performed.

The mechanical behaviour of material during heat treatment might be significantly affected by possible phase transformation of metal intrinsic structure. In fact, this phenomenon represents one of the greatest problems in heat treatment modelling. Considering, however, that AISI 316L austenite stainless steel we deal with, is characterized by high chrome and nickel content which suppresses phase transformation and keeps the material fully austenite from the melting point to room temperature [10], there is no need for phase transformation to be included in our mathematical model.

2 DETERMINATION OF MATERIAL BEHAVIOUR PARAMETERS

Mechanical material properties for AISI 316L stainless steel were determined by considering the results of an experiment, presented in [10]. The test called "Satoh test" was performed there to validate the constitutive equation used for welding simulation and, as in our case, to determine temperature dependent mechanical properties. The considered constitutive model and identified parameters were further validated on examples of deep drawing intermediate annealing and post welding heat treatment.

Only some material properties are given explicitly in [10] (temperature dependent Young's modulus, expansion coefficient and initial yield stress), the rest of temperature dependent mechanical material properties (material hardening and viscous properties) are determined by the inverse identification method based computer code developed in our laboratory [14] and [15]. Thermal material properties (specific heat and thermal conductivity) and density were acquired from literature [16].

2.1 Mechanical Properties Identification

The aim of the Satoh test is to reproduce in a simplified way the thermo-mechanical cycle that occurs in heat affected zone during welding. The test is considered to be one-dimensional with homogeneous stress and temperature fields. The sample, constrained to move unidirectionally, is subjected to prescribed temperature cycles loading. From the measured time dependent force stress can be calculated. To allow investigation of viscosity effects different cooling rates (0.3°C/s, 10°C/s and air cooling) were imposed [10]. The experiment in [10] is well described and a sufficient amount of experimental results is given, which allows us to reproduce the experiment numerically and identify the missing mechanical

material properties. The assumed material behaviour is isotropic, with linear and temperature dependent hardening. The equivalent stress - equivalent plastic strain curve is thus given by the following relation

$$\sigma(T)=\sigma_0(T)+H(T)\cdot\gamma, \quad (4)$$

where σ, σ_0, H and γ are respectively the equivalent stress, the yield stress, the hardening modulus and the equivalent plastic strain. The results of the performed inverse identification are given in Table 1, where hardening modulus H, viscous material data A and n are presented, while strain rate sensitivity parameter m in Eq. (3) is set to zero. For the temperature values not given in the table a linear interpolation between the tabulated values is applied.

Table 1. *Identified material properties*

T [°C]	H [MPa]	A [(MPa^{n}s)$^{-1}$]	n [/]
20	1788	1.00×10^{-22}	2.0
490	1805	1.00×10^{-20}	2.5
550		6.00×10^{-20}	4.8
620		3.13×10^{-16}	4.9
680		2.01×10^{-18}	5.2
720		3.65×10^{-15}	4.4
760		6.52×10^{-16}	5.0
850	757	3.31×10^{-15}	5.3
900		7.88×10^{-14}	5.1
920		5.90×10^{-17}	4.9
930		4.45×10^{-11}	3.3
1100	231	7.50×10^{-09}	3.3
1125		4.98×10^{-08}	2.0

3 VALIDATION CASES

Adequacy of both, the adopted viscous-elastic-plastic constitutive model and the performed material parameters identification, is validated by numerically simulating two significant industrial cases: (i) the intermediate annealing between two consecutive drawing sequences of a deep drawn stainless pan and (ii) the stress relieving of a plate subject to simplified welding experiment.

3.1 Case 1: Simulation of Two-stage Deep Drawing with Intermediate Annealing

In a drawn part the deep drawing process produces deformations and stresses which can be of such a magnitude that they can induce significant damage and can even tear the product. In some cases an intermediate stress relieving, i.e. annealing of the formed workpiece before its exposure to the subsequent forming operation is needed to prevent undesired rupture. In the considered case study the mechanical consequences of the annealing are modelled, employing the previously described viscous-elastic-plastic material model. The performed simulation clearly proves that during annealing, the residual stresses converge towards zero, but they do not disappear totally. The rate of convergence depends on the annealing process parameters and on the material itself.

The task of the investigated deep drawing problem is to draw an axi-symmetrical pot of 288 mm diameter and 145 mm depth (H) with the undrawn rim of 50 mm width (Fig. 1). Since the focus of the article is not on the metal forming process the particularities, such as friction conditions, blank holding force, kinematics of the tools and material behaviour of the blank sheet, are omitted.

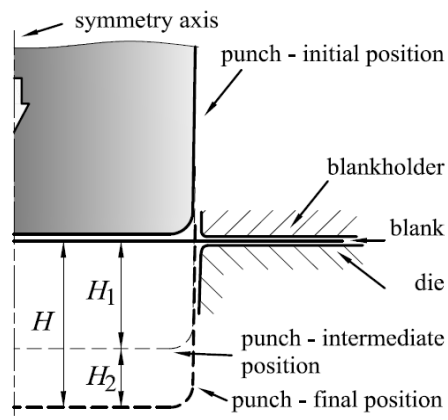

Fig. 1. *Scheme of the drawing operation*

Because of severe stresses that originate during drawing, the pot cannot be drawn in a single step. In consequence, the total punch stroke of H = 145 mm is divided into two strokes of H_1 = 100 mm and H_2 = 45 mm, respectively, with the intermediate annealing which enables drawing of the second stroke without tearing the pot.

Annealing was conducted in a vacuum kiln to avoid metallurgical changes of stainless steel. Due to low pressure of the remaining gas, the heat is transferred in a kiln mainly by radiation. The temperature of the hot body, in Fig. 2 designated as

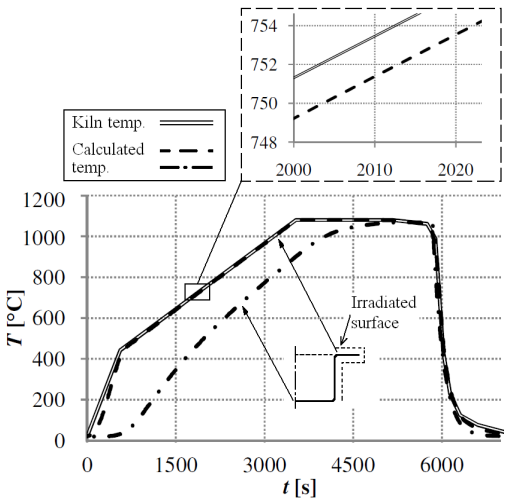

Fig. 2. *Measured kiln temperature and simulated temperature variations in the pot by annealing*

Kiln temp., was recorded and considered in the numerical simulation of the annealing. Not all the pot's surfaces were, however, exposed to irradiation; namely, by putting several pots in line to be annealed simultaneously in the kiln, certain surfaces fall into shadow. Accordingly, only the rim of the pot and the external surface of the cylindrical wall were irradiated in the numerical simulation, while the bottom of the pot was held in shadow (Fig. 2). The temperature rise of the bottom is mainly due to heat conduction transferring heat from the side wall into the bottom. For both specific zones the simulated temperature variations are displayed in Fig. 2. Except for the initial stage, the temperature of the irradiated section (dashed line) follows practically the kiln temperature with a time delay of just 10 s; whereas the temperature evolution at the pot's bottom (dash-dot line) is delayed for approximately 1000 s due to the above described boundary conditions. At the end of the annealing process the pressure inside the kiln was raised and the door was opened causing a rapid change of the temperature inside the kiln. In the numerical model this was considered by adding convection heat transfer mode with ambient temperature of 20°C and estimated convective heat transfer coefficient $h = 7$ W/Km on all the surfaces of the pot.

Since the geometry and loading of the investigated deep drawing problem are axi-symmetric while the material properties are assumed isotropic, the problem can be modelled as axi-symmetrical one. The initial geometry of the stainless steel blank is circular with diameter of 500 mm and thickness of 0.7 mm.

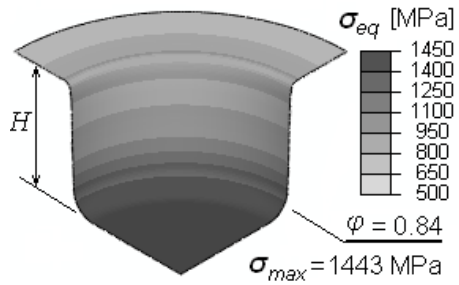

Fig. 3. *Mises equivalent stress distribution and maximal equivalent plastic strain in the case of a single stroke deep drawing simulation*

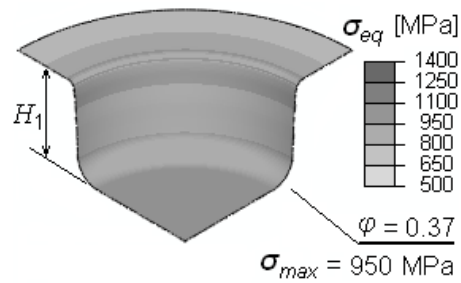

Fig. 4. *Mises equivalent stress distribution and maximal equivalent plastic strain after the first partial stroke (before annealing)*

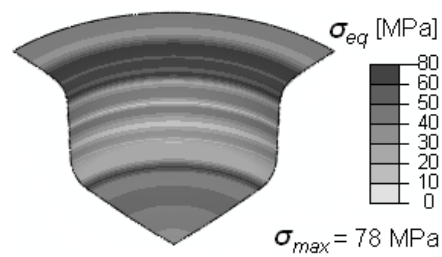

Fig. 5. *Mises equivalent stress distribution after the first partial stroke (after annealing)*

Two comparative numerical studies of the considered deep drawing problem are to be presented in the sequel. In the first, the blank is drawn to its maximal depth $H = 145$ mm in one single step. The obtained results, shown in Fig. 3, indicate that the equivalent stress σ_{eq} and the equivalent plastic strain φ are so high that, according to our experience with similar problems, tearing of the pot is most likely to occur.

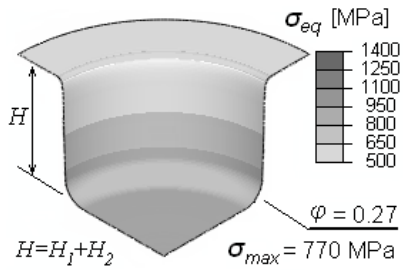

Fig. 6. *Mises equivalent stress distribution and maximal equivalent plastic strain after the second stroke*

The stress field plots in Fig. 3, as well as those plotted in Figs. 4 to 6, are the membrane stresses given at the instance of the accomplished punch stroke with the tools not yet removed. Since local bending stresses are removed from the represented stress distribution the state actually refers to the sheet mid-surface.

The results of the deep drawing simulation performed in two stages with intermediate annealing are shown in Figs. 4 to 6. The stress state of the formed part after the first draw to the depth of 100mm is shown in Fig. 4. From the stress distribution in Fig. 5, which refers to the situation obtained after exposure of the same formed part to annealing, a great amount of stress relieving can be observed. But, contrary to common engineering thought, the annealed stresses are not zero. They remain at significant, non negligible value. Besides the stress reduction, the ductility of the blank is also restored, thus enabling further plastic deformation. The stress state in the product after the second stroke is shown in Fig. 6. As expected, the extreme values of the resulting equivalent stress and equivalent plastic strain are significantly smaller than in the case of a single stroke drawing (Fig. 3).

3.2 Case 2: Simulation of Post Weld Heat Treatment

This case study reported in [10], refers to a rectangular (250·160 mm^2) stainless steel plate of 10mm thickness, supported in four points, and a single pass weld with no filler metal made in the longitudinal direction along the centreline of the plate (Fig. 7a). The applied welding process parameters in the experiment were $U = 10$ V, $I = 150$ A, the travelling speed of the moving heat source being 0.677 mm/s. The temperature at several points on the upper and lower surface of the plate, and the displacement of the plate under the fusion line were continuously measured.

To perform a computer simulation of the considered thermo-mechanical process a three-dimensional solid finite element model is built. Due to the plate symmetry and symmetry of the applied heat loading only one half of the plate is modelled, with *z-x* plane being a symmetry plane. The numerical model consists of 8768 eight-node brick finite elements with linear edgewise interpolation of displacement and temperature degrees of freedom. In modelling the heat source and thermal boundary conditions we follow the guidelines considered in [10]. Fluid flow in the molten pool due to the electric arc and convective effects, which both intensify heat transfer in the pool, was considered only approximately. With regard to the thermal conductivity of solid metal at 1000 °C the respective value of thermal conductivity of the solid finite elements representing the molten pool is assumed twice as large.

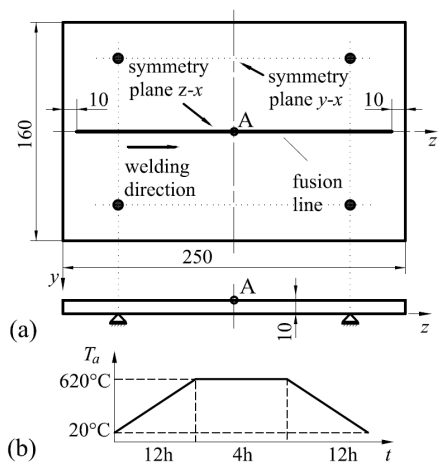

Fig. 7. *Sheet plate subject to moveable heat source: (a) plate geometry, (b) prescribed ambient temperature in the kiln during heat treatment*

The results of the welding simulation performed by considering the thermo-mechanical coupling in a staggered way prove full reliability of the built numerical model, here included the adopted constitutive model and performed material characterisation. Field distributions of the residual normal stresses in the longitudinal (z) and transverse (y) direction after welding, computed on the upper surface of the plate, are shown in Figs. 8 b and d.

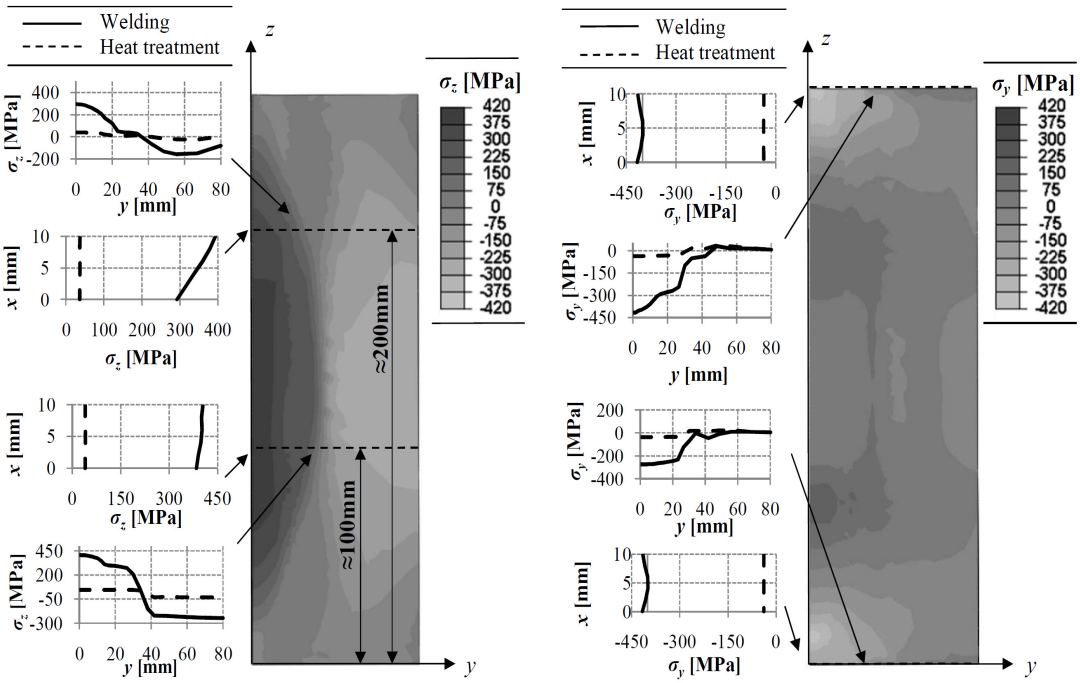

Fig. 8. *Computed normal residual stresses after welding and subsequent annealing*

Maximal tensile longitudinal residual stresses are around 13% overestimated compared to the calculated results in [10], whereas other values of residual stresses differ for less than 10%. Since it is no physical justification to assert that the numerical results regarding residual stresses in [10] are correct, we can only conclude that our results are qualitatively in satisfactory agreement with the compared reference ones. In fact, despite not being acquainted with a large part of material parameters used in [10] and adopting different constitutive model in our simulation, the obtained results give full confidence of both, the adopted viscous-elastic-plastic constitutive model and the inversely numerically identified material parameters.

Trustworthiness of the numerical model gained through the simulation of heat treatment conditions in welding of the plate could now be tested with regard to annealing of the existing residual stresses after welding. The temperature evolution of the process is governed by the furnace internal ambient temperature, which is prescribed by the graph, given in Fig. 7b. Stress relieving heat treatment regime can be divided in three sequences: i) slow heating of the furnace from room temperature to temperature T_a = 620 °C, ii) maintaining constant temperature for a specified period, and iii) slow cooling to room temperature T_a = 20 °C. The same mechanical boundary conditions as applied in the welding simulation are adopted.

The residual stress state obtained after the described annealing procedure is mild compared to the stresses before annealing, which can be observed from the respective graphs of normal stresses displayed in Figs. 8 a and c. After heat treatment the welding residual stresses are reduced to approximately 5 to 10% of their initial value. Both tensile and compressive stress peaks are significantly reduced. The amount of the manifested stress reduction in the considered case agrees well with the stress reduction of similar cases given in [11]. This amount depends mostly on the annealing temperature, holding time and residual stress state before heat treatment. The latter means, that the rate of stress reduction (in percents) is greater for high residual stresses than for low stresses. But the annealed stress state of a material particle with high pre-annealing stress still remains higher than the annealed stress of a material particle with low pre-annealing stress.

Progressive reduction of residual stress σ_z during annealing process for point A is shown in Fig. 9. Although a considerable drop of residual stress can be observed already from the very beginning of the heating, the biggest decrease happens above 550 °C. In spite of holding at high temperatures for a rather long time, residual stresses do not drop to zero as it is commonly adopted by many engineers, see Fig 9, Figs. 8 a and c.

As it was reported in [5], no additional plastic strain is produced during the cooling stage of the heat treatment process. This fact was confirmed by the model considered in our study.

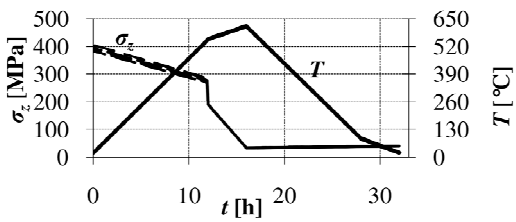

Fig. 9. *Residual stress reduction during annealing process (point A in Fig. 7a)*

4 CONCLUSION

In general, and especially when technological processes at elevated temperatures are addressed, numerical simulations require proper constitutive modelling in order to be physically objective. Above all, potential models must consider viscous component of the material behaviour. Next, not of lesser importance is assurance of true values for the material parameters involved in constitutive models. This is not a trivial task in case of temperature dependence.

In our investigation, mechanical material parameters of austenite stainless steel 316L (AISI) were characterised upon experimental data given in [10]. Validation of the adopted thermo-mechanical constitutive model and respective material parameters was performed by numerical simulation of the heat treatment process by annealing of residual stresses originated after welding. In general, good agreement between numerical simulations and data from literature was established. Another example with the thermo-mechanical modelling required was a deep drawing case with intermediate annealing process needed in order to successfully accomplish the prescribed forming. Again, to obtain a reliable numerical simulation of such processes, proper material modelling and a consistent set of material parameters is of crucial importance.

It can be concluded that with a proper set of material parameters even a relatively simple constitutive model, such as the power law model employed in ABAQUS [13], can be appropriate for numerical simulations of thermo-mechanical processes where either severe inhomogeneous or relatively homogeneous thermo-mechanical fields evolve, e.g. welding and annealing processes. Finally, we should, however, not forget that the adopted constitutive model is applicable only for steels with no phase transformations, which means that the model does not consider an additional volume change due to possible martensite transformation.

5 REFERENCES

[1] Sinha, A.K. *Physical Metallurgy Handbook*, McGraw-Hill Handbooks, New York [etc.], 2003.

[2] Tyrkiel, E.J. *Heat Treating*, vol. 1, no. 2, 1979, p. 52-54.

[3] Thelning, E.K. *Steel and Its Heat Treatment*, Butterworths, London, 1984.

[4] Ronda, J., Oliver, G.J. Comparison of applicability of various thermo-viscoplastic constitutive models in modelling of welding. *Comput Methods Appl Mech Engrg*, 1997 (153), p. 195-221.

[5] Wang, J., Lu, H., Murakawa, H. Mechanical behaviour in local post weld heat treatment, *JWRI*, 1998 (27), p. 83-88.

[6] Alberg, H., Berglund, D. Comparison of plastic, viscoplastic, and creep models when modelling welding and stress relief heat treatment, *Comp. Methods Appl. Mech. Engrg*, 2003 (196), p. 5189-5208.

[7] Josefsson, B.L. Residual stresses and their redistribution during annealing of a girth-butt welded thin walled pipe, *J. Pressure Vessel Technol*, 1982 (104), p. 245-250.

[8] Berglund, D., Alberg, H., Runnehalm, H. Simulation of welding and stress relief heat treatment of an aero engine component, *Finite element in analysis and Design*, 2003 (39), p. 865-881.

[9] Lemaitre, J., Chaboche, J.L. *Mechanics of Solid Material*, Cambridge University Press, Canbridge, England, 1990.

[10] Depradeux, L., Jullien, J.F. Numerical simulations of thermomechanical phenomena during tig welding and experimental validation on analytical tests of increasing complexity. In: Cerjak, H., Bhadeshia, H.K.D.H., Kozeschnik, E., (Eds.): *Mathematical modelling of weld phenomena 7*, Technische Universität Graz, 2005, p. 269-294.

[11] Totten G.E., Bates C.E., Clinton N.A. *Handbook of Quenchants and Quenching Technology*, Chapter1-Introduction to the heat treating of steel, ASM International Materials Park, OH, 1993, p. 1-33.

[12] Mole, N., Bobovnik, G., Kutin, J., Štok, B., Bajsić, I., An improved three-dimensional coupled fluid-structure model for Coriolis flowmeters. *J. fluids struct*., 2008 (24), p. 559-575.

[13] ABAQUS, 2007. User Manual, Version 6.7

[14] Koc, P., Štok, B. Computer-aided identification of the yield curve of a sheet metal after onset of necking, *Computational Materials Science*, 2004 (31), p. 155-168.

[15] Koc, P., Štok, B. (2008) Usage of the yield curve in numerical simulations, *Strojniški vestnik - Journal of Mechanical Engineering,*vol. 54, p. 821-829.

[16] Richter, F. *Stahleisen-Sonderberichte*, Heft 8. Verlag Stahleisen M. B. H., Düsseldorf.